

# Gradient-free online learning of subgrid-scale dynamics with neural emulators

H. Frezat<sup>1,2,3\*</sup>, R. Fablet<sup>3</sup>, G. Balarac<sup>1,4</sup>, and J. Le Sommer<sup>2</sup>

<sup>1</sup>Univ. Grenoble-Alpes, CNRS UMR LEGI, Grenoble, France

<sup>2</sup>Univ. Grenoble-Alpes, CNRS, IRD, G-INP, INRAE, IGE, Grenoble, France

<sup>3</sup>IMT Atlantique, CNRS UMR Lab-STICC, INRIA Team Odyssey, Brest, France

<sup>4</sup>Institut Universitaire de France (IUF), Paris, France

## Key Points:

- Parametrizations learned with online approaches are known to be more stable but require differentiable solvers.
- We train a differentiable emulator of the reduced solver that enables online approaches for the parametrization.
- This opens new avenues to learn stable parametrizations for non-differentiable legacy codes.

---

\*<https://hrkz.github.com>

Corresponding author: Hugo Frezat, [hugo.frezat@gmail.com](mailto:hugo.frezat@gmail.com)

## Abstract

In this paper, we propose a generic algorithm to train machine learning-based subgrid parametrizations online, i.e., with a posteriori loss functions, but for non-differentiable numerical solvers. The proposed approach leverages a neural emulator to approximate the reduced state-space solver, which is then used to allow gradient propagation through temporal integration steps. We apply this methodology on a single layer quasi-geostrophic system with topography, known to be highly unstable in around 500 temporal iterations with offline strategies. Using our algorithm, we are able to train a parametrization that recovers most of the benefits of online strategies without having to compute the gradient of the original solver. It is demonstrated that training the neural emulator and parametrization components separately with different loss quantities is necessary in order to minimize the propagation of approximation biases. Experiments on emulator architectures with different complexities also indicates that emulator performance is key in order to learn an accurate parametrization. This work is a step towards learning parametrization with online strategies for weather models.

## Plain Language Summary

Systems used to predict climate and weather dynamics are composed of large code-bases developed from a long effort of multiple teams of individuals. In order to speed-up the computation, one use a subgrid parametrization that models the transfers at the smallest scales. While machine learning has been a promising alternative to train such model, these are known to be subject to instabilities and are thus not usable in practice. An alternative approach called “online” trains the model using the solver’s trajectory, and is thus more accurate while ensuring stability. However, this approach requires numerical derivatives of the model, which are not available in the case of large earth systems and would require significant human effort to be implemented. In this paper, we train a neural emulator that approximates the solver dynamics while being differentiable, allowing for the online approach to be used. Even if an emulator is used instead of the true solver, the parametrization is able to remain close to the reference parametrization. Before only limited to toy system, this research enables training accurate and stable models for realistic systems.

## 1 Introduction

Numerical models used for simulating the evolution of fluid flows generally require subgrid scales (SGS) and physical parameterizations. These serve the purpose of representing the impact of scales that remain unresolved by the discretized solver as for instance subgrid turbulent processes (Rogallo & Moin, 1984; Meneveau & Katz, 2000). They may also account for other physical phenomena that are not explicitly accounted for by the partial differential equations. SGS and physical parameterizations are generally considered to be key components of numerical models in Earth System science (Fox-Kemper et al., 2019; Schneider et al., 2017). In these numerical models, they are often rate-controlling components which largely govern the long term behavior of model solutions (Maher et al., 2018; Hewitt et al., 2020). This is why significant efforts are concentrated on the development of SGS and physical parameterizations in these communities. Machine learning (ML) techniques have now been widely applied to SGS and physical parameterizations for numerical simulations, as already discussed in reviews (Brunton et al., 2020; Vinuesa & Brunton, 2022). These ML-based components have been demonstrated in different applications, including atmospheric circulation (Rasp et al., 2018; Yuval & O’Gorman, 2020), oceanic circulation (Bolton & Zanna, 2019; Guillaumin & Zanna, 2021), and sea-ice dynamics (Finn et al., 2023) but also with benchmarks of toy models (Ross et al., 2023). The ambition of this emerging field is to design hybrid numerical models that improves upon existing ones by combining physics-based PDE solvers and ML-based trainable components. In this framework, well-constrained aspects are incorporated into the resolved equations, while components that are less rigorously constrained or follow a statistical behavior are represented by ML-based algorithms. When possible, physical knowledge can also be incorporated in the ML-based component (Pawar et al., 2023; Frezat et al., 2021; Beucler et al., 2021). Hybrid numerical models are currently designed through an optimization procedure that attempts to improve its ability to replicate the results of a higher fidelity model. In practice, higher fidelity means that it can reproduce additional physical processes (e.g., microphysics) (Seifert & Rasp, 2020), contains information from reanalyses (McGibbon & Bretherton, 2019; Watt-Meyer et al., 2021) or from higher resolutions (Frezat et al., 2022). The hybrid numerical models are typically run at coarser resolution and the parameters of their ML components are optimized in order to fit a given training objective. This objective is usually formulated from pre-existing high-resolution, process resolving numerical models (that is direct numerical simulation

(DNS), or high-resolution version of the same code) but also from observations or lab experiments. By essence, this optimization is very much related to the tuning of model parameters, or to the estimation of state-dependent correction of models.

Several recent results suggest that ML-based SGS parametrization give better results when the ML components are trained with online strategies (Sirignano et al., 2020; MacArt et al., 2021; Duraisamy, 2021; Sirignano & MacArt, 2023; Pahlavan et al., 2024). The training of ML components for hybrid numerical models is said to use an online strategy if the evaluation of the training objective involves integrating the hybrid numerical model for several time steps. Note that the same idea has also been referred to as *a posteriori* (Frezat et al., 2022), solver-in-the-loop (List et al., 2022), differentiable (Shankar et al., 2023; Fan & Wang, 2024) or end-to-end in the ML community. In practice, the strategy has been shown to lead to more stable simulations, with better performance in *a posteriori* tests. However, the online strategy typically requires to compute the derivative of the hybrid numerical model with respect to the parameters of the ML components. These results suggest that, as in other fields of physical science, the emerging paradigm of differentiable programming shows great potential for the design of hybrid numerical models applied to the simulations of turbulent systems. Differentiable programming (DP) is often combined with automatic differentiation (AD) which allows to automatically obtain the derivatives of a chain of operations in order to be used in an optimization procedure based on a gradient descent variant. AD frameworks are typically implemented by specific libraries or programming languages, and have seen many new development applications in physical sciences (Um et al., 2020; Holl et al., 2020; Heiden et al., 2021; Négier et al., 2023). There has been a particularly active community around the problem of turbulence modeling (Dresdner et al., 2022; Kochkov et al., 2021; Takahashi et al., 2021) and climate-geoscientific modeling (Gelbrecht et al., 2023; Wagner et al., 2023; Ramadhan et al., 2020).

However, most numerical models are usually not easily differentiable. This major practical issue makes the optimization of ML components with online strategies difficult. For performance and historic reasons, legacy codes used in production are written in low-level programming languages such as Fortran or C. This is the case in many physics community including for Earth System models used for climate projections. These hand-optimized numerical models are also relatively large codebases ( $\sim$  hundreds of thousands of lines of codes) and would thus require lots of effort to be re-implemented in a modern AD lan-

guage. Generating adjoints automatically using code analysis libraries is possible, but practically complicated to deploy and lead to suboptimal codes (in particular in terms of memory footprint). In practice, online learning strategies are thus not easily amenable with production scale codes. Different approaches that includes the temporal aspect provided by online learning have also been proposed and rely on gradient-free optimization algorithms. While gradient-free optimization is a large subfield, we identify two large families that have recently seen many applications to training large ML models in the context of hybrid physical models. First, methods adapted from data assimilation (Pawar & San, 2021; Huang et al., 2022) and inverse problems as for instance the ensemble Kalman inversion (EKI) (Iglesias et al., 2013; Kovachki & Stuart, 2019; Lopez-Gomez et al., 2022). More recently, many studies applying gradient-free policy search in reinforcement learning (RL) have been explored in particular for turbulence modeling (Kim et al., 2022; Kurz et al., 2023; Novati et al., 2021; Bae & Koumoutsakos, 2022). Overall, it is not clear which strategy performs best or should be preferred in practical situations.

Alternatively, we here propose to leverage neural emulation as a strategy to perform online supervised learning while avoiding the need for a differentiable solver. The use of neural emulators also connects with some algorithms in the field of simulation based inference which use neural networks to solve inverse problems (Cranmer et al., 2020) and the field of data assimilation for model error correction (Bocquet, 2023; Nonnenmacher & Greenberg, 2021). Here, the neural emulator aims at approximating the full solver in the (reduced) model state space. We can rephrase the neural emulation as an approximation of the temporal evolution of some PDE. We describe in this paper a generic algorithm which allows to train jointly a ML-based SGS parametrization for a non-differentiable solver with an online strategy and a neural emulator of the same solver. To overcome bias separation between the two components, we introduce a two-step procedure and a compensated loss function that isolates the different training objectives. The algorithm is implemented and demonstrated to produce stable models on a challenging subgrid parametrization problem. We also show that we are able to recover most of the benefits of online strategies without having to compute the gradient of the reduced resolution solver.

The paper is structured as follows: in Section 2, we outline the general issue being addressed and its particular application to SGS modeling. Section 3 describes the two-step algorithm that allows training a SGS parametrization with online strategy using a differentiable neural emulator of the target solver. In Section 4, we describe our

evaluation benchmark, consisting of a two-dimensional quasi-geostrophic system subject to kinetic energy backscatter. The performance of our approach is then illustrated in Section 5 and discussed in Section 6.

## 2 Problem statement

As explained in the introduction, training a model online requires the ability to compute the gradient of the loss function with respect to model parameters, which involves solver calls and consequently also requires its gradient. Let us define a typical regression task where one would seek to minimize a cost between some prediction  $\hat{\mathbf{z}} = \mathcal{M}(\mathbf{y} | \theta)$  and ground truth of the same input space  $\mathbf{z}$ , i.e.

$$\arg \min_{\theta} \mathcal{L}(\mathbf{z}, \mathcal{M}(\mathbf{y} | \theta)). \quad (1)$$

During the training process, the parameters of  $\mathcal{M}$ ,  $\theta$  are optimized in order to minimize  $\mathcal{L}$ . The minimization algorithm requires the computation of the gradient of the loss function with respect to the trainable parameters  $\theta$ ,

$$\frac{\partial \mathcal{L}}{\partial \theta}(\mathbf{z}, \mathcal{M}(\mathbf{y} | \theta)) = \left( \frac{\partial \mathcal{M}(\mathbf{y} | \theta)}{\partial \theta} \right)^{\top} \frac{\partial \mathcal{L}}{\partial \mathcal{M}}. \quad (2)$$

In practice,  $\mathcal{M}$  could be a simple operator from which the analytical gradient would be computed beforehand and provided to the optimization process. However, in differentiable solvers, we are interested in the temporal evolution of a system  $E(\mathbf{y}) : \mathbb{R}^n \rightarrow \mathbb{R}^n$  of a vector-valued quantity of interest  $\mathbf{y}(t)$ . In a discretized formulation, the operator  $E$  is typically defined by a sequence of operations,

$$\mathbf{y}(t + \Delta t) = E_p \circ \dots \circ E_1(\mathbf{y}(t)). \quad (3)$$

Now, if  $\mathcal{M} \equiv E$ , the required partial derivative of the system is defined as a Jacobian in the minimization formulation (2),

$$\frac{\partial E_i}{\partial \theta} = \begin{bmatrix} \frac{\partial E_{i,1}}{\partial \theta_1} & \dots & \frac{\partial E_{i,1}}{\partial \theta_n} \\ \vdots & \ddots & \vdots \\ \frac{\partial E_{i,m}}{\partial \theta_1} & \dots & \frac{\partial E_{i,m}}{\partial \theta_n} \end{bmatrix} \quad (4)$$

for a single step of the temporal evolution operator  $E$ . Composing the partial derivatives of the sequences of operators in  $E$  can be done by applying the chain rule,

$$\frac{\partial E}{\partial \theta} = \frac{\partial (E_p \circ \dots \circ E_1)}{\partial \theta} = \frac{\partial E_p}{\partial E_{p-1}} \dots \frac{\partial E_2}{\partial E_1} \frac{\partial E_1}{\partial \theta} \quad (5)$$

The gradient of  $E$  can quickly become difficult to maintain by hand. Note that when training NNs, it is required to have a scalar-valued loss function  $\mathcal{L}$ , which means that its derivative is a gradient instead of a Jacobian. The way partial derivatives are computed is called reverse-mode differentiation (Baydin et al., 2018), which here consists of a series of vector-matrix multiplications starting from

$$\left( \frac{\partial \mathcal{L}}{\partial \mathcal{M}} \right)^\top \frac{\partial E_p}{\partial \theta} : \mathbb{R}^n. \quad (6)$$

Solving (5) can be as trivial as implementing a solver leveraging automatic differentiation (AD) languages or libraries. However, as pointed out in the introduction, this is a challenging task for large-scale solvers such as GCMs that would require a lot of development work and might lead to the vanishing gradient problem (Hochreiter, 1998) due to many function compositions.

## 2.1 The specific SGS modeling problem

Here, we are interested in modeling small-scale quantities arising in differential equations restricting the grid resolution and thus the performance of the simulations (Sagaut, 2005). We assume an underlying differential equation involving the time evolution of variables  $\mathbf{y}(t)$  to be known and defined by a direct operator  $f(\mathbf{y})$ . The aim is to solve an equivalent approximation for reduced variables  $\bar{\mathbf{y}}(t)$  such that

$$\begin{cases} \frac{\partial \mathbf{y}}{\partial t} = f(\mathbf{y}), & \mathbf{y} \in \Omega \\ \frac{\partial \bar{\mathbf{y}}}{\partial t} = g(\bar{\mathbf{y}}) + \mathcal{M}(\bar{\mathbf{y}}), & \bar{\mathbf{y}} \in \bar{\Omega} \\ \mathcal{T}(\mathbf{y}) = \bar{\mathbf{y}} \end{cases} \quad (7)$$

where  $\bar{\Omega} \subset \Omega$ ,  $g$  is a reduced operator,  $\mathcal{M}$  is a SGS model and  $\mathcal{T}$  is a projection that maps direct variables to reduced ones. The objective is formulated as an inverse problem where operator  $\mathcal{M}$  has to be determined such that the evolution of the reduced variables match the projection  $\mathcal{T}(\mathbf{y})$  of the direct variables  $\mathbf{y}$ . In most situations, we have  $f = g$  with variables existing on different spaces or dimensionalities. Note that this can be applied to any type of partial differential equation without any loss of generality. Within a learning framework, one states the identification of a general reduced term

$$\tau(\mathbf{y}) = \mathcal{T}(f(\mathbf{y})) - g(\mathcal{T}(\mathbf{y})) \approx \mathcal{M}(\bar{\mathbf{y}} | \theta) \quad (8)$$

where  $\theta$  are trainable model parameters. Under the assumption that  $\mathcal{T}$  commutes with partial derivatives, the classical approach comes to train a model  $\mathcal{M}(\bar{\mathbf{y}} | \theta)$  as a functional

approximation of the missing term  $\tau(\mathbf{y})$ . The classical strategy to optimize  $\mathcal{M}$  is to generate a dataset  $\mathbb{D} = \{\bar{\mathbf{y}}\} \rightarrow \{\tau(\mathbf{y})\}$  that maps input states  $\bar{\mathbf{y}}$  to the SGS term  $\tau(\mathbf{y})$  beforehand and then finding optimal parameters  $\theta$  offline, i.e., without any knowledge of the dynamics  $\partial\bar{\mathbf{y}}/\partial t$  during training. Here, let us refer to an offline loss  $\mathcal{L}_{\text{off}}$ , the corresponding minimization problem (1) writes

$$\arg \min_{\theta} \mathcal{L}_{\text{off}} = \arg \min_{\theta} \ell_{\text{off}}(\tau(\mathbf{y}), \mathcal{M}(\bar{\mathbf{y}} | \theta)) \quad (9)$$

where  $\ell_{\text{off}}$  is an instantaneous scalar-valued loss function  $\ell_{\text{off}} : (\mathbb{R}^d, \mathbb{R}^d) \rightarrow \mathbb{R}$  that penalizes the NN prediction from the expected missing term. In this context,  $\mathcal{M}$  is defined as a NN implemented in a standard deep learning framework such as PyTorch or TensorFlow. This allows for the computation of the gradient of the loss function, i.e., injecting (9) in (2),

$$\frac{\partial \mathcal{L}_{\text{off}}}{\partial \theta} = \left( \frac{\partial \ell_{\text{off}}}{\partial \mathcal{M}} \right)^{\top} \frac{\partial \mathcal{M}(\bar{\mathbf{y}} | \theta)}{\partial \theta}. \quad (10)$$

Using this formulation, the problem is simple to setup since both terms on the right-hand side are automatically determined using AD capabilities. However, while the offline approach is efficient to accurately reproduces the statistical properties of the missing term  $\tau(\mathbf{y})$ , it has been shown to lead to unstable simulations in non-linear, chaotic dynamical systems such as those found in turbulence modeling (Maulik et al., 2019). Improving the stability of the SGS model can be done by increasing the size of the dataset, in particular by reducing the inter-sample correlation (Guan et al., 2022) or adding physics-based terms in the loss function (Guan et al., 2023). As pointed out in (Frezat et al., 2022), the offline training approach may not be able to optimize a model based on relevant metrics in the context of a dynamical system. An equivalent training approach tailored to this task, called online, has already been explored successfully in turbulence modeling (Um et al., 2020; Holl et al., 2020; MacArt et al., 2021). Formally, (Frezat et al., 2022) described the minimization problem (1) of the online loss  $\mathcal{L}_{\text{on}}$ ,

$$\arg \min_{\theta} \mathcal{L}_{\text{on}} = \arg \min_{\theta} \ell_{\text{on}}(\{\mathbf{y}(t)\}_{t \in [t_0, t_1]}, \{\Phi_{\theta}^t(\bar{\mathbf{y}}(t_0))\}_{t \in [t_0, t_1]}) \quad (11)$$

where  $\Phi$  is the flow operator that advances the reduced variables in time using the currently training model  $\mathcal{M}$ ,

$$\Phi_{\theta}^t(\bar{\mathbf{y}}(t_0)) = \bar{\mathbf{y}}(t_0) + \int_{t_0}^t g(\bar{\mathbf{y}}(t')) + \mathcal{M}(\bar{\mathbf{y}}(t') | \theta) dt' \quad (12)$$

and  $\ell_{\text{on}}$  is a temporal scalar-valued loss function  $\ell_{\text{on}} : (\mathbb{R}^{d \times B}, \mathbb{R}^{d \times B}) \rightarrow \mathbb{R}$  defined on  $B$  timesteps that discretizes the temporal interval  $[t_0, t_1]$ . Let us expand the gradient of



the online loss  $\mathcal{L}_{\text{on}}$  from (2) at final time  $t_1$ ,

$$\frac{\partial \mathcal{L}_{\text{on}}}{\partial \theta} = \left( \frac{\partial \ell_{\text{on}}}{\partial \Phi_{\theta}^t} \right)^{\top} \frac{\partial \Phi_{\theta}^t}{\partial \theta}(\bar{\mathbf{y}}(t_0)) = \left( \frac{\partial \ell_{\text{on}}}{\partial \Phi_{\theta}^t} \right)^{\top} \left( \int_{t_0}^t \frac{\partial g(\bar{\mathbf{y}}(t'))}{\partial \theta} + \frac{\partial \mathcal{M}(\bar{\mathbf{y}}(t') | \theta)}{\partial \theta} dt' \right). \quad (13)$$

This process requires the ability to compute the partial derivatives of the reduced solver  $g$  with respect to the trained model parameters  $\theta$ , i.e.  $\partial g / \partial \theta$ . Here we are interested in determining this quantity such that  $\tau$  can be learnt online without re-implementing  $g$  using an AD framework.

### 3 Coupled SGS-emulation

Building on (Nonnenmacher & Greenberg, 2021), we propose a learning scheme that is able to jointly train a differentiable emulator of  $g$  and its corresponding SGS term. Let us introduce a differentiable emulator  $\mathcal{E}$  of  $g$

$$\mathcal{E}(\bar{\mathbf{y}}) \approx g(\bar{\mathbf{y}}), \text{ s.t. } \frac{\partial \mathcal{E}}{\partial \theta} \text{ is known.} \quad (14)$$

This differentiability condition is automatically fulfilled if  $\mathcal{E}$  is implemented using AD capabilities. It is possible to define  $\mathcal{E}$  as a trainable neural emulator, which involves training its parameters  $\Theta$  simultaneously with the SGS model parameters  $\theta$ . Substituting into (11),

$$\arg \min_{\Theta, \theta} \mathcal{L}_{\text{on}} = \arg \min_{\Theta, \theta} \ell_{\text{on}} \left( \{\mathbf{y}(t)\}_{t \in [t_0, t_1]}, \{\bar{\mathbf{y}}(t_0) + \int_{t_0}^t \mathcal{E}(\bar{\mathbf{y}}(t') | \Theta) + \mathcal{M}(\bar{\mathbf{y}}(t') | \theta) dt'\}_{t \in [t_0, t_1]} \right). \quad (15)$$

We recall here that the final goal of this learning scheme is to provide a stable SGS model  $\mathcal{M}$  that will be used for forward simulations with the reduced solver  $g$ . However, with the coupled formulation (15), the model  $\mathcal{M}$  is not explicitly restricted to represent SGS dynamics only. Indeed the learning scheme jointly optimizes  $\Theta$  and  $\theta$  such that  $\mathcal{E} + \mathcal{M}$  approximates the direct solver  $f$ . There is therefore no guarantee that  $\theta$  will be optimal for  $\mathcal{M}$  to represent the SGS term.

#### 3.1 Joint neural SGS-emulation learning

It is possible to penalize both the neural emulator and the SGS model by composing the loss function such that  $\ell = \ell^{\mathcal{E}}(\mathcal{E}(\bar{\mathbf{y}} | \Theta)) + \ell^{\mathcal{M}}(\mathcal{M}(\bar{\mathbf{y}} | \theta))$  where  $\ell^{\mathcal{E}}$  and  $\ell^{\mathcal{M}}$  targets the neural emulator and SGS model, respectively. It might be possible to use filtering operations to identify their effect on high-resolution reference data, but their respective definitions may not be simple to implement and might not include inter-scale

transfers. Instead, we propose a two-step online formulation that trains  $\mathcal{E}$  and  $\mathcal{M}$  sequentially,

**Step 1 (neural emulator):**

$$\arg \min_{\Theta} \ell_{\text{on}}^{\mathcal{E}} \left( \{\bar{\mathbf{y}}(t)\}_{t \in [t_0, t_1]}, \{\bar{\mathbf{y}}(t_0) + \int_{t_0}^t \mathcal{E}(\bar{\mathbf{y}}(t') | \Theta) dt'\}_{t \in [t_0, t_1]} \right), \quad (16)$$

**Step 2 (subgrid-scale model):**

$$\arg \min_{\theta} \ell_{\text{on}}^{\mathcal{M}} \left( \{\mathbf{y}(t)\}_{t \in [t_0, t_1]}, \{\bar{\mathbf{y}}(t_0) + \int_{t_0}^t \mathcal{E}(\bar{\mathbf{y}}(t')) + \mathcal{M}(\bar{\mathbf{y}}(t') | \theta) dt'\}_{t \in [t_0, t_1]} \right). \quad (17)$$

These two steps are formulated using an online learning strategy, but (16) minimizes a loss for an integration of the reduced solver  $g$  while (17) is equivalent to the classical online SGS formulation (11) with  $\mathcal{E} \approx g$ . This sequential training scheme does not require a differentiable version of the reduced solver  $g$ . Indeed, let us factor the modified flows  $\varphi$  appearing on the right-hand side of (16) and (17) respectively,

$$\varphi_{\Theta}^t(\bar{\mathbf{y}}(t_0)) = \bar{\mathbf{y}}(t_0) + \int_{t_0}^t \mathcal{E}(\bar{\mathbf{y}}(t') | \Theta) dt', \quad (18)$$

$$\varphi_{\theta}^t(\bar{\mathbf{y}}(t_0)) = \bar{\mathbf{y}}(t_0) + \int_{t_0}^t \mathcal{E}(\bar{\mathbf{y}}(t')) + \mathcal{M}(\bar{\mathbf{y}}(t') | \theta) dt'. \quad (19)$$

Then, expanding again the gradient of the online losses using (2) yields,

$$\left( \frac{\partial \ell_{\text{on}}^{\mathcal{E}}}{\partial \varphi_{\Theta}^t} \right)^{\top} \frac{\partial \varphi_{\Theta}^t}{\partial \Theta}(\bar{\mathbf{y}}(t_0)) = \left( \frac{\partial \ell_{\text{on}}^{\mathcal{E}}}{\partial \varphi_{\Theta}^t} \right)^{\top} \left( \int_{t_0}^t \frac{\partial \mathcal{E}(\bar{\mathbf{y}}(t') | \Theta)}{\partial \Theta} dt' \right), \quad (20)$$

$$\left( \frac{\partial \ell_{\text{on}}^{\mathcal{M}}}{\partial \varphi_{\theta}^t} \right)^{\top} \frac{\partial \varphi_{\theta}^t}{\partial \theta}(\bar{\mathbf{y}}(t_0)) = \left( \frac{\partial \ell_{\text{on}}^{\mathcal{M}}}{\partial \varphi_{\theta}^t} \right)^{\top} \left( \int_{t_0}^t \frac{\partial \mathcal{E}(\bar{\mathbf{y}}(t'))}{\partial \theta} + \frac{\partial \mathcal{M}(\bar{\mathbf{y}}(t') | \theta)}{\partial \theta} dt' \right) \quad (21)$$

with  $\mathcal{E}$ ,  $\mathcal{M}$  are arbitrary NNs implemented using AD and  $\ell_{\text{on}}^{\mathcal{E}}$ ,  $\ell_{\text{on}}^{\mathcal{M}}$  loss functions also defined within the machine learning framework, supporting AD by construction.

### 3.2 Neural emulator error compensations

In theory, our two-step learning scheme would be equivalent to the classical online SGS learning scheme with a differentiable solver if and only if  $\mathcal{E} \equiv g$ . In practice however, the neural emulator will only represent an approximation of the reduced solver, i.e.,  $\mathcal{E} \approx g$ . The performance of the SGS training (17) thus strongly relies on the emulator's ability to reproduce the adjoint (see. [Ouala et al. \(2023\)](#) for an example) of the reduced dynamics on a given time horizon  $[t_0, t]$ . The instantaneous emulation mismatch between the solver and emulator can be expressed as

$$\varepsilon(\bar{\mathbf{y}}) = g(\bar{\mathbf{y}}) - \mathcal{E}(\bar{\mathbf{y}}). \quad (22)$$

In practice, the loss function (17) always acts on reduced resolution, i.e., it takes the projection  $\mathcal{T}$  on direct resolution data  $\mathbf{y}(t)$ . Substituting the projected reduced term (8) on the left-hand side gives the "exact" reduced flow,

$$\mathcal{T}(\mathbf{y}(t)) = \mathcal{T}\left(\mathbf{y}(t_0) + \int_{t_0}^t f(\mathbf{y}(t')) dt'\right) = \bar{\mathbf{y}}(t_0) + \int_{t_0}^t g(\bar{\mathbf{y}}(t')) + \tau(\mathbf{y}(t')) dt' \quad (23)$$

Now, expanding the modified flow  $\varphi_{\theta}^t(\bar{\mathbf{y}}(t_0))$  with the emulation mismatch in the right-hand side of (17), we see that if  $\mathcal{M}$  approximates  $\tau$ , the flow is equivalent only if  $\epsilon$  vanishes,

$$\varphi_{\theta}^t(\bar{\mathbf{y}}(t_0)) = \bar{\mathbf{y}}(t_0) + \int_{t_0}^t g(\bar{\mathbf{y}}(t')) - \epsilon(\bar{\mathbf{y}}(t')) + \mathcal{M}(\bar{\mathbf{y}}(t') | \theta) dt' \quad (24)$$

It is clear here that the emulation mismatch  $\epsilon$  will be absorbed by the SGS model  $\mathcal{M}$  during its training phase, since  $\mathcal{E}$  is already fixed. In order to optimize  $\mathcal{M}$  against  $\tau$  using this standard online loss function, it is important that the emulation mismatch remain small. Controlling this mismatch is challenging in particular due to the temporal integration. Recall that the loss function  $\ell_{\text{on}}^{\mathcal{M}}$  is defined on a sequence of states of the system  $\bar{\mathbf{y}}(t)$  but never involves the missing SGS term  $\tau$  that  $\mathcal{M}$  is trying to learn. We instead propose to re-target the loss function  $\ell_{\text{on}}^{\mathcal{M}}$  so that it directly operates on the subgrid-scale terms for the considered time window,

$$\ell_{\text{on}}^{\mathcal{M}_{\text{subgrid}}}(\{\mathbf{y}(t)\}_{t \in [t_0, t_1]}, \{\varphi_{\theta}^t(\bar{\mathbf{y}}(t_0))\}_{t \in [t_0, t_1]}) = \ell_{\text{on}}^{\mathcal{M}}(\{\tau(\mathbf{y}(t))\}_{t \in [t_0, t_1]}, \{\mathcal{M}(\varphi_{\theta}^t(\bar{\mathbf{y}}(t_0)))\}_{t \in [t_0, t_1]}) \quad (25)$$

In practice, this loss acts at time  $t$  as a model composition of the bias emulation mismatch  $\epsilon$ ,

$$\mathcal{M}(\varphi_{\theta}^t(\bar{\mathbf{y}}(t_0))) = \mathcal{M}(g(\bar{\mathbf{y}}(t)) - \epsilon(\bar{\mathbf{y}}(t)) + \mathcal{M}(\bar{\mathbf{y}}(t))) \quad (26)$$

Here, the first benefit is that model  $\mathcal{M}$  is now trained to be invariant to the emulator mismatch  $\epsilon$  with respect to the SGS term  $\tau$ . The second benefit comes from the small-scale target of the loss function, absorbing the large-scale emulator mismatch  $\epsilon$  into a small-scale error. From experiments, we observed that penalizing the SGS terms in the loss function largely reduces the large-scale ambiguities from the emulation mismatch  $\epsilon$  while maintaining the online behavior of the learning strategy, since these quantities are still evaluated over a temporal horizon  $[t_0, t]$ . From now, we will refer to the original loss  $\ell_{\text{on}}^{\mathcal{M}}$  as "state"-based online loss and the re-targeting loss  $\ell_{\text{on}}^{\mathcal{M}_{\text{subgrid}}}$  as "subgrid"-based online loss. Experiments based on emulators in the next section will be designed on the subgrid loss, since training with the original state loss did not lead to stable mod-

**Algorithm 1** Two-step online SGS (model) learning scheme

---

**input:** reduced dataset  $\{\bar{\mathbf{y}}(t)\}$  computed from  $g$   
**input:** solver dataset  $\{\mathbf{y}(t), \tau(\mathbf{y}(t))\}$  computed from  $f$   
**input:** emulator architecture and parameters  $\mathcal{E}(\Theta \sim \mathcal{N})$   
**input:** model architecture and parameters  $\mathcal{M}(\theta \sim \mathcal{N})$

// STEP 1: NEURAL EMULATOR, EQ. (16)

**while** emulator parameters not converged **do**  
     randomly select a temporal interval:  $t = [t_0, t_1]$   
     initialize from reduced states:  $\hat{\mathbf{y}}(t_0) = \bar{\mathbf{y}}(t_0)$   
     integrate the emulator using ODE solver:  $\{\hat{\mathbf{y}}(t)\}_{t \in [t_0, t_1]} = \text{ODE}(\mathcal{E}(\hat{\mathbf{y}}(t_0) | \Theta))$   
     optimize emulator parameters on "state" loss:  $\ell_{\text{on}}^{\mathcal{E}}(\{\bar{\mathbf{y}}(t)\}_{t \in [t_0, t_1]}, \{\hat{\mathbf{y}}(t)\}_{t \in [t_0, t_1]})$   
**end while**

// STEP 2: SUBGRID MODEL,  $\Theta$  FIXED, EQ. (17)

**while** model parameters not converged **do**  
     randomly select a temporal interval:  $t = [t_0, t_1]$   
     initialize from projected direct states:  $\hat{\mathbf{y}}(t_0) = \mathcal{T}(\mathbf{y}(t_0))$   
     integrate system using ODE solver:  $\{\hat{\mathbf{y}}(t)\}_{t \in [t_0, t_1]} = \text{ODE}(\mathcal{E}(\hat{\mathbf{y}}(t_0)) + \mathcal{M}(\hat{\mathbf{y}}(t_0) | \theta))$   
     optimize model parameters on "subgrid" loss:  $\ell_{\text{on}}^{\mathcal{M}_{\text{subgrid}}}(\{\mathbf{y}(t)\}_{t \in [t_0, t_1]}, \{\hat{\mathbf{y}}(t)\}_{t \in [t_0, t_1]})$   
**end while**

**output:** optimized model parameters  $\mathcal{M}(\theta)$

---

els. The discretized version of the two-step learning scheme, suitable for numerical applications (detailed below), is outlined in Algorithm 1.

#### 4 Application: quasi-geostrophic dynamics

In turbulent flows, the energy cascade drives energy from the large scales to the small scales until molecular viscous dissipation (forward-scatter), but the inverse transfer called backscatter in which energy is transferred from the small scales back to the large scales (Lesieur & Metais, 1996) is also in play, particularly for geophysical flows. This is explained by the relative dominance of the Coriolis force which creates vortical structures that appear two-dimensional. Historically, developing SGS models that account for backscatter is a challenging task (Piomelli et al., 1991; Schumann, 1995; Liu et al., 2011). Indeed, an overprediction of backscatter that can not be compensated by eddy-viscosity will lead to an accumulation of small-scale energy causing simulations to become numerically unstable. In two-dimensional flows, we observe a dual cascade composed of "forward" enstrophy and "inverse" energy, in a statistical sense. As a consequence, a large number of SGS models have been proposed in particular for geophysical flows (see Danilov et al. (2019) for a review) with well-documented configurations and performance metrics (Fox-Kemper & Menemenlis, 2008). SGS modeling is also a key issue for the simulation of ocean

and atmosphere dynamics because of the large range of motions involved (Jansen et al., 2015; Juricke et al., 2019, 2020; Frederiksen et al., 2012). As a case study framework, we consider barotropic QG flows. While providing an approximate yet representative system for rotating stratified flows found in the atmosphere and ocean dynamics, it involves relatively complex SGS features that make the learning problem non-trivial. As such, QG flows are regarded as an ideal playground to explore and assess the relevance of machine learning strategies for SGS models in geophysical turbulence. The governing equations of direct vorticity  $\omega$  for the QG model with bottom topography  $\eta$  are

$$\frac{\partial \omega}{\partial t} + \mathcal{N}(\omega + \eta, \psi) = \nu \nabla^2 \omega - \mu \omega - \beta \partial_x \psi + F_\omega, \quad (27)$$

$$\nabla^2 \psi = -\omega \quad (28)$$

where  $\mathcal{N}(\omega + \eta, \psi) = \partial_x \psi \partial_y (\omega + \eta) - \partial_y \psi \partial_x (\omega + \eta)$  is the non-linear vorticity advection,  $\nu$  is the viscosity,  $\mu$  is a large-scale drag coefficient,  $\beta$  is the Earth rotation vector approximation by beta-plane and  $F_\omega$  is an additional source term. Now, the derivation of the reduced system for QG dynamics follows the same procedure that is typically used for fluid dynamics turbulence modeling (also called large-eddy simulation). The projection operator  $\mathcal{T}$  at spatial coordinate  $\mathbf{x}$  is here given as a discretization (or coarse-graining)  $\mathcal{D} : \Omega \rightarrow \bar{\Omega}$  and the convolution of  $\omega$  with a kernel function  $G(\mathbf{x})$  (Leonard, 1975),

$$\bar{\omega}(\mathbf{x}) = \mathcal{D} \left( \int G(\mathbf{x} - \mathbf{x}') \omega(\mathbf{x}') d\mathbf{x}' \right). \quad (29)$$

We can then derive the equations which govern the evolution of reduced vorticity  $\bar{\omega}$ ,

$$\frac{\partial \bar{\omega}}{\partial t} + \mathcal{N}(\bar{\omega} + \bar{\eta}, \bar{\psi}) = \nu \nabla^2 \bar{\omega} - \mu \bar{\omega} - \beta \partial_x \bar{\psi} + \underbrace{\mathcal{N}(\bar{\omega} + \bar{\eta}, \bar{\psi}) - \overline{\mathcal{N}(\omega + \eta, \psi)}}_{\tau_\omega} + \bar{F}_\omega \quad (30)$$

where  $\tau_\omega$  is the SGS term. In this context,  $\tau_\omega$  can not be determined from the reduced variables because of the non-linear interactions of small-scale dynamics  $\overline{\mathcal{N}(\omega + \eta, \psi)}$  and must thus be statistically modeled in order to close equation (30).

#### 4.1 Simulation setup

In order to study the learning problem, we solve equations (27)-(28) using a pseudospectral code with full 3/2 dealiasing (Canuto et al., 2007) and a classical fourth-order explicit Runge Kutta time advancement. The system is defined in a squared domain  $\Omega, \bar{\Omega} = [-\pi, \pi]^2$ , or domain length  $L = 2\pi$  discretized with a Fourier basis, i.e. double-periodic boundary conditions on  $N$  and  $\bar{N}$  grid points with uniform spacing and a grid ratio  $\Delta' =$

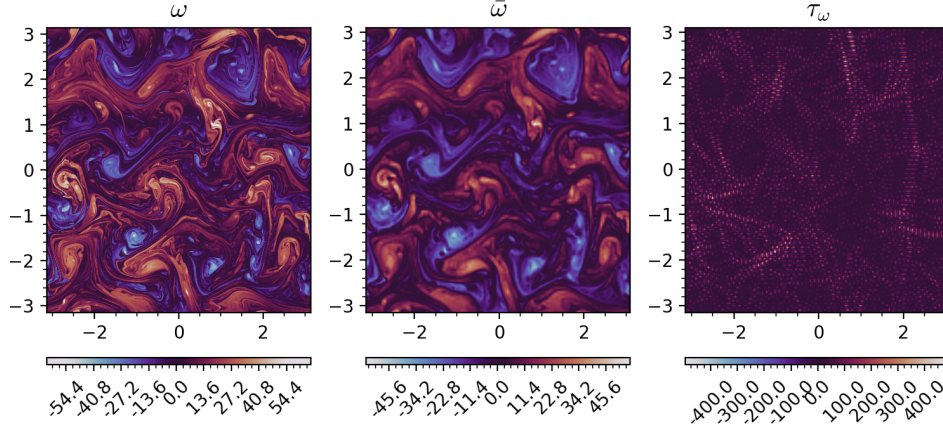


**Figure 1.** Direct vorticity fields  $\omega$  (left), reduced vorticity fields  $\bar{\omega}$  (middle) and SGS term  $\tau_\omega$  (right) at the end of a testing horizon (24000 temporal iterations) from the direct simulation using  $f$ .

$N/\bar{N} > 1$  between direct and reduced solver resolutions. We extract the SGS term with spatial filtering (29) using a spectral cut-off filter  $G$  and sample non-residual quantities along the simulations, i.e.  $\{\omega \rightarrow \tau_\omega\}$  is obtained from direct solver  $f$  and  $\{\bar{\omega}\}$  is obtained from reduced solver  $g$ . We energize the system using a wind-forced configuration representative of mesoscale oceanic simulation (Graham & Ringler, 2013). We produce an equilibrium solution from a slowly varying in time circular source at large scale  $k$  with steady enstrophy rate injection  $\langle F_\omega(t)^2 \rangle = 3$  such that

$$F_\omega(t) = \cos(4y) - \cos(4x + \pi \sin(1.5t)). \quad (31)$$

We modify the configuration and add unaligned sinusoidal bumps topography (Thompson, 2010) in order to create interesting dynamics with significant nonzonal components in jets induced by the Coriolis force. Stationary turbulent states are obtained from random Gaussian initialization  $\omega(t=0) \sim \mathcal{N}(0,1)$  at moderate wavenumbers  $k \in [10, 32]$ , followed by a 500000 iterations spin-up on a smaller grid ( $1024^2$ ) and energy propagation to the smallest scales of the direct grid ( $2048^2$ ) in about 25000 iterations. We show examples of vorticity fields and SGS term in Fig. 1.

## 4.2 Learning setup

To generate the corresponding datasets suitable for online learning, we need continuous trajectories and thus subsample at each iteration from  $g$  for (16) and every  $\Delta'$  iterations

from  $f$  for (17) so that these states directly correspond to one iteration performed by  $g$ . For the SGS model  $\mathcal{M}$  (both online and emulator-based), we use a simple standard CNN with  $\sim 923\text{K}$  learnable parameters from 10 convolution layers with kernels of size 5 and 64 filters each, followed by non-linear Relu activations. This architecture has been shown to be able to learn extremely accurate SGS dynamics in (Frezat et al., 2022). For the large-scale dynamics represented by the neural emulator  $\mathcal{E}$ , we explore a state-of-the-art neural architecture and a simpler CNN in order to assess the impact of the emulation quality on the SGS learning:

- **Dilated Residual Network (DRN).** The architecture combines residual networks with the encode-process-decode paradigm (Sanchez-Gonzalez et al., 2018) and dilated convolutions, recently applied to different types of flows (Stachenfeld et al., 2022) and defined with  $\sim 581\text{K}$  learnable parameters.
- **Convolutional Neural Network (CNN).** The architecture is equivalent to the CNN used for the SGS model except that we have  $\sim 616\text{K}$  learnable parameters from 7 convolution layers.

Note that for each of these architectures, input boundaries are replicated periodically given the geometry of the domain. Using state of the art architectures for the SGS model could further improve the overall performance and might be interesting to explore. However, we may point out that the goal is not to design an optimal NN-based architecture but rather to evaluate the training strategy at the same SGS computational cost during evaluation stage. Concerning the functional loss  $\ell$ , we restricted ourselves to simple MSE both for the neural emulator and the SGS model,

$$\ell_{\text{off}}(\cdot, \hat{\cdot}) = \ell_{\text{on}}^{\mathcal{E}}(\cdot, \hat{\cdot}) = \ell_{\text{on}}^{\mathcal{M}_{\text{subgrid}}}(\cdot, \hat{\cdot}) = \frac{1}{B} \sum_{b=1}^M \frac{1}{D} \sum_{d \in D} (\cdot_d^b - \hat{\cdot}_d^b)^2 \quad (32)$$

where  $B$  corresponds to either the batch size during offline learning or the number of temporal iterations during online learning and  $D$  is the number of grid points  $d$  in the domain. While using the MSE led to satisfying results here, we note that with the online approach, time-averaged quantities such as spectra, transfers or distributions could be used to improve performance of the neural emulator and/or SGS model further, depending on the target application.

**Table 1.** Parameters of the numerical setup for simulation (top) and learning (bottom).

Note that reduced systems use the same parameters, except for grid resolution  $\bar{N}$  and timestep  $\bar{\Delta t} = \Delta' \Delta t$ . The quantities are given in numerical (dimensionless) as directly used in the solver for reproducibility.

Simulation parameter		
Length of the domain	$L$	$2\pi$
Linear drag	$\mu$	$2 \times 10^{-2}$
Kinematic viscosity	$\nu$	$1.025 \times 10^{-5}$
Rossby parameter	$\beta$	$2.195 \times 10^2$
Topography	$\eta$	$\sin(3y) + \cos(3x)$
Timestep	$\Delta t$	$10^{-4}$
Number of grid points	$N$	2048
Grid ratio	$\Delta'$	16
Learning parameter		
offline batch size / online iterations	$B$	25
Training trajectories		10
Testing trajectories		5
Samples per trajectory		3000
Number of trainable parameters		

## 5 Results

We generate simulation data and train corresponding models using parameters summarized in Table. 1. The objective here being to design a stable and efficient SGS model, we compare the results of our two-step algorithm with several baselines.

**Online model (reference).** The main objective here is to reproduce the performance of the online model implemented using a differentiable solver using our two-step strategy that does not require differentiability. We also explore the performance of the online reference model trained with the "subgrid" loss in Appendix 1.



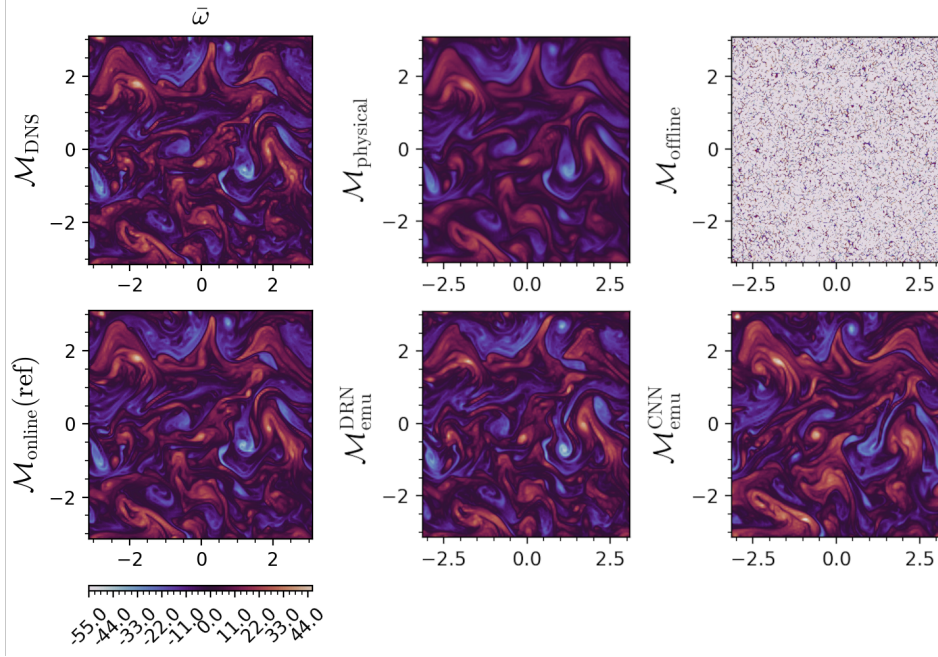


**Figure 2.** Reduced vorticity fields  $\bar{\omega}$  after a short simulation run of 500 reduced temporal iterations (8000 equivalent direct iterations) comparing reference filtered DNS (top-left) and differentiable online strategy (bottom-left) with baselines (top-middle,right) and emulation-based models (bottom-middle,right).

**Offline model.** We train a SGS model using the classical offline strategy with the same CNN architecture, as described above. This model is known to be unstable and motivates the advantages of the online strategy.

**Physical model.** As a common baseline, we also use the Smagorinsky model (Smagorinsky, 1963), defined as an eddy coefficient proportional to the resolved strain rate  $\bar{S}$  with the dynamic procedure proposed by (Germano et al., 1991; Lilly, 1992) to compute  $C_s$  and apply spatial averaging with positive clipping (Pawar et al., 2020; Guan et al., 2022) in order to avoid locally negative constants  $C_s(x, y) < 0$ , i.e. ensuring that the models are purely diffusive and  $\nu_e \geq 0$ ,

$$\tau_{\omega} = \nabla \cdot \underbrace{[(C_s \Delta)^2 |\bar{S}|]}_{\nu_e} \nabla \bar{\omega}. \quad (33)$$

### 5.1 SGS model evaluation

We first run a new simulation from a different random initial conditions with our ref-

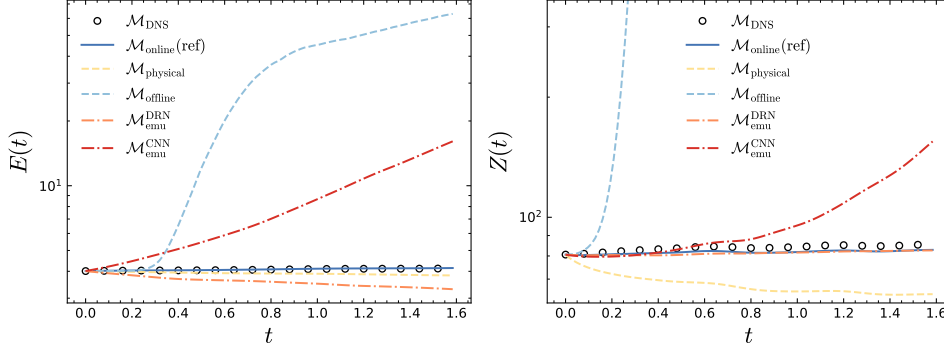


**Figure 3.** Domain-averaged invariants energy  $E(t)$  (left) and enstrophy  $Z(t)$  (right) after a short simulation run of 1000 reduced temporal iterations (16000 equivalent direct iterations).

ferences, baselines and SGS models trained using the two-step algorithm using both the CNN and DRN architectures. Recall that evaluations are now run with the reduced solver  $g$  and a SGS model  $\mathcal{M}$ , except for the direct reference  $\mathcal{M}_{\text{DNS}}$  that uses direct solver  $f$ .

We show in Fig. 2 the final vorticity fields  $\bar{\omega}$  after 500 reduced temporal iterations. It is first clear here that the offline learning strategy does not lead to a stable model in this configuration, and that numerical blowup characterized by a point-by-point noisy vorticity field happens quickly. On the opposite, the physical model is too diffusive, completely removing small-scale features and the associated dynamics.

We can also validate that the online strategy is indeed a stable and accurate model to represents the SGS dynamics in QG systems, as it is remarkably close to the DNS.

Concerning the neural emulators, they both remain stable over this temporal horizon. However, we can already see that both emulator-based models start to differ from the reference.

To understand the time-evolution of the flow statistics, we look at the invariants of the QG equations in Fig. 3, in the limit of inviscid flows (Bouchet & Venaille, 2012) for energy

$$E(t) = \frac{1}{2} \int \mathbf{u}(t)^2 \, dr \quad (34)$$

and enstrophy

$$Z(t) = \frac{1}{2} \int \omega(t)^2 \, dr. \quad (35)$$

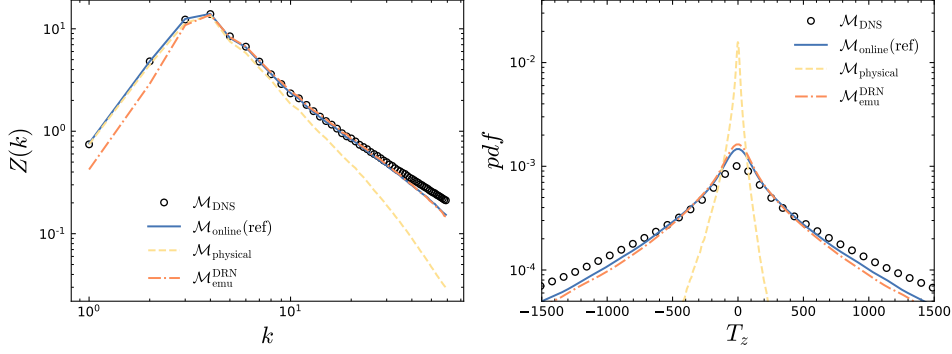


**Figure 4.** Time-averaged enstrophy spectrum (left) and final probability distribution of the enstrophy transfer term (right) for 5 trajectories of longer simulation runs of 2000 temporal iterations (32000 equivalent direct iterations).

We can confirm previous observations concerning accumulation of enstrophy from the offline model, exponentially growing until blowup. We also clearly observe the over-dissipation of enstrophy for the physical model. Both neural emulators show enstrophy evolution relatively close to the references on the first 500 temporal iterations, with DRN-based emulator model being almost equivalent to the reference online model on the entire temporal horizon. While small scales are well represented by the models trained from the neural emulators, it is apparent that they are not as efficient on the large scales, as seen by the constant increase of energy for the CNN-based emulator model that will eventually lead to a numerical blowup. The DRN-based model does not accumulate energy but performs slightly worse than the physical model.

Integrating over a longer temporal horizon composed of 2000 reduced iterations, we can inspect the statistical behavior of the different models in Fig. 4. First, we verify that the enstrophy spectrum

$$Z(k) = \int_{|\mathbf{k}|=k} |\omega(\mathbf{k})|^2 dS(\mathbf{k}). \quad (36)$$

and integrated modeled transfers

$$\int \bar{\omega} \tau_{\omega} dS = \int (\bar{\mathbf{u}} \bar{\omega} - \bar{\mathbf{u}} \bar{\omega}) \cdot \nabla \bar{\omega} dS = - \int T_Z dS. \quad (37)$$

of the online (differentiable reference) correctly reproduces the dynamics of the DNS. At this point, both the offline model and the CNN-based emulator model failed due to accumulation energy at small and large scale, respectively. On the left, we note a good agreement of the physical model at the smallest wavenumbers but excessive dissipation at the

largest wavenumbers. The DRN-based emulator model is extremely accurate on the largest wavenumbers which corresponds with the term used in the "subgrid" loss function during training,  $\tau_\omega$  acting mostly on the smallest scales. The DRN-based emulator model is however not as accurate on the smallest wavenumbers. This might be improved by training with an large-scale additional term in the loss function such as velocity  $\mathbf{u}$  or stream-function  $\psi$ . On the right, it is clear that the modeled transfers distribution produced by the physical model has a large peak and a poor reproduction of the distribution tails. On the other hand, the DRN-based model is efficient at maintaining a modeled transfers distribution close to the references.

We again recall that experiments with SGS models trained from neural emulators with the state loss rather than the subgrid loss have been omitted from these plots because of their unstable behavior.

## 5.2 Neural emulator performance

We want here to identify the stability difference and better understand the source of error between models obtained from neural emulators of different complexities, mostly in terms of NN architecture and corresponding number of trainable parameters.

We look at the evolution of the root-mean-squared error (rms) of some reference  $\cdot$  and predicted  $\hat{\cdot}$  quantities over temporal integration steps  $B$ ,

$$\ell_{\text{rms}}(\cdot, \hat{\cdot}) = \frac{1}{\sigma(\cdot)B} \sqrt{\frac{1}{D} \sum_{d \in D} (\cdot_d - \hat{\cdot}_d)^2} \quad (38)$$

where  $\sigma$  is the standard deviation.

In Fig. 5, we show the  $\ell_{\text{rms}}$  of different SGS models compared to the DNS. First, vorticity mismatch indicates that each model is able to improve substantially compared to the reduced simulation without SGS models (or  $\mathcal{M}_0$ ). In particular, NN-based models produce an error that increases slower than the physical models. The emulator-based models are performing slightly worse than the reference online model but remain competitive. The velocity mismatch is quite different, since error for the CNN-based emulator model grows faster and is already larger than the one without SGS model. For the DRN-based model, the error is still large compared to the other models, but already improves substantially. It is clear here that there is still some progress to be made about

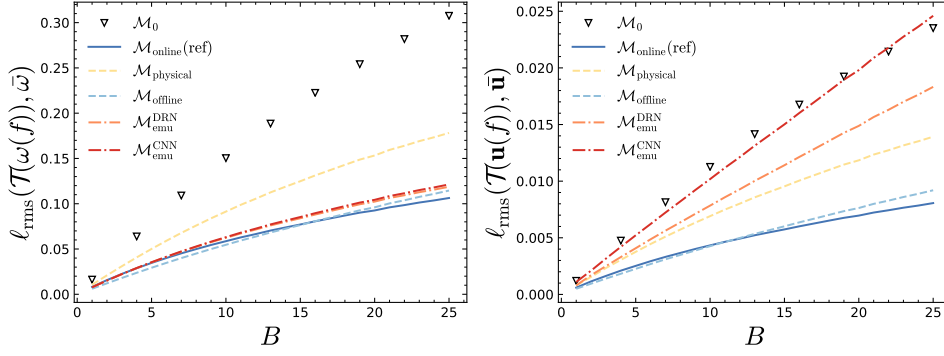


**Figure 5.**  $\ell_{\text{rms}}$  normalized by the number of temporal integration steps  $B$  for the vorticity  $\omega$  (left) and velocity  $\mathbf{u}$  (right). The error for each SGS model is computed against the DNS. As for comparison, we also show the reduced simulation without model ( $\mathcal{M}_0$ ) that is known to be unstable.

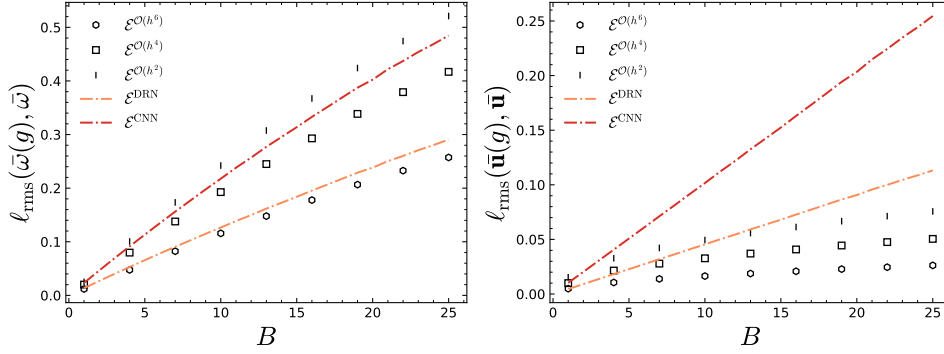


**Figure 6.**  $\ell_{\text{rms}}$  compared to the reduced DNS, normalized by the number of temporal integration steps  $B$  for the reduced vorticity  $\bar{\omega}$  (left) and velocity  $\bar{\mathbf{u}}$  (right) for NN-based emulators and finite difference discretization of different orders.

the emulator-based predictions on the largest scales, potentially induced by some error bias in the neural emulator.

We isolate the error produced by the neural emulators compared to the solver at reduced resolution in Fig. 6. In addition to the neural emulators, we show the error produced by finite difference (FD) schemes (or emulators) of different orders from  $h^2$  to  $h^6$  using modified wavenumbers in a spectral method (Kravchenko & Moin, 1997). We can confirm that the error produced by the neural emulators is mainly affected by large scales. Indeed, the vorticity error of the DRN-based model is equivalent to a 6th order FD scheme, while the CNN-based emulator model performs slightly worse than a 4th order FD but

better than the 2nd order FD. However, both produce velocity errors larger than a 2nd order FD.

This further confirms that improvements on the large-scale predictions of the neural emulator are potentially a limitation that must be addressed.

## 6 Discussion

In this article, we have proposed an algorithm for training an online ML-based SGS parametrization, i.e., with *a posteriori* criteria for non-differentiable numerical solvers. The core idea of our approach is to use neural emulators that represent the reduced dynamics, equivalent to the original equations in a lower dimensional space. These emulators are by definition differentiable and allows us to train the parametrization in an online setting. The main benefit of our two-step algorithm is to avoid error compensation between the emulator and the trained ML-based parametrization using different loss targets for the SGS model and for the neural emulator, respectively. Indeed, as described in Subsection 3.2 above, learning jointly emulator and parametrization will lead to error compensation, where the parametrization-part accomodates the imperfect nature of the emulator-part. When used in a simulation, the trained parametrization is found to add spurious large scale transfers that decreases overall performance.

Our two-step algorithm has been tested on a two-dimensional SGS modeling problem and shows performance levels close to those obtained with online learning on differentiable solvers on small-scale metrics. In a highly turbulent quasi-geostrophic setting with bottom topography, the model trained with our two-step algorithm is able to remain stable over many temporal iterations. Moreover, it has a matching performance with the online model in terms of small-scale quantities, and overall enstrophy spectrum and transfers distribution. Nonetheless, additional work will be required in order to alleviate some systematic biases in the SGS model associated with the inherently imperfect nature of the neural emulator. This error is mostly visible at large scale. We think that constraining the loss function of the neural emulator on related large scale quantities such as velocities instead of vorticity could further improve its performance, translating to a smaller bias in the learned SGS model.

This work represents a first step toward more complex neural emulators. While the experimental system used here has a considerable amount of state parameters, more work

will still be required for deploying our approach with full complexity physical models. We have also seen that the SGS learning step is sensitive to the quality of the neural emulator, which could be a potential issue when emulating larger numerical systems. However, we are optimistic that improving the performance of the emulator is technically possible, as we have already seen large improvements between two neural architectures. At this stage, it is also unclear how our algorithm compares with other existing gradient free training techniques. In particular, it would be informative to perform a comparison with the approach described in (Pedersen et al., 2023) that proposes to use neural emulation to map model states at different future times in order to train SGS parametrizations.

Our neural emulator approach is not only relevant for SGS parametrization but also more generally for differentiable computing, with a large potential in Earth System Modeling (Gelbrecht et al., 2023). Our emulation-based approach could be leveraged for similar tasks as for instance for calibrating model parameters (Wagner et al., 2023) or learning model error (Farchi et al., 2021). Our algorithm could also provide a practical solution for deploying variational data assimilation (DA) techniques without having to compute the adjoint of the direct solver (Carrassi et al., 2018). In practice, variational DA frameworks requires an adjoint operator which is complicated to maintain. Adjoint-free minimization techniques have been proposed, including ensemble methods (Yang et al., 2015) but trades-off performance and computing time. In previous work (Nonnenmacher & Greenberg, 2021) and recent applications to different tasks, differentiable emulation opens a possible alternative approach for variational DA of numerical models. Neural emulation therefore appears as a strategy to further explore in order to develop hybrid climate models that leverage the full potential of differentiable programming.

## Appendix A Re-targeting loss without emulation mismatch

We have discussed the unstable behavior of the online "state" loss when emulator mismatch is present. In order to better understand the performance impact of the re-targeting "subgrid" loss, we train a new reference model using the differentiable solver and the "subgrid" loss. The learning setup for this model is the same as described in Sec. 4.2. We show two indicators of performance in Fig. A1. On the left, the "state" loss is shown to be more accurate than the "subgrid" loss at reproducing the temporal evolution of domain-averaged energy, although the difference is small (see scale). On the right, the enstrophy spectrum is also closer for the "state" loss. This is not surprising since the

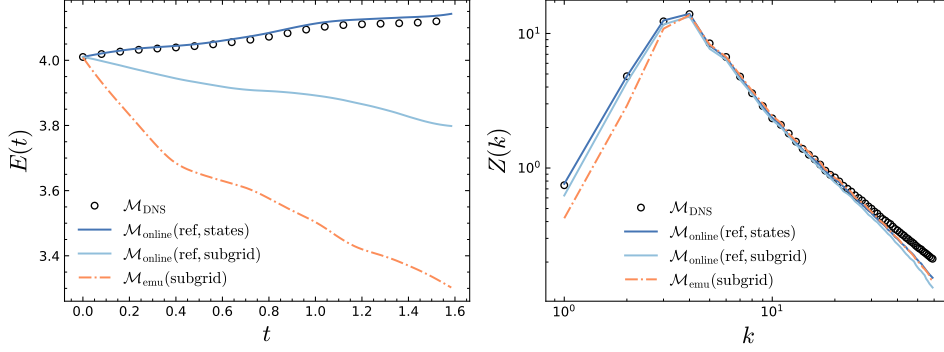


**Figure A1.** Domain-averaged invariants energy  $E(t)$  (left) and time-averaged enstrophy spectrum (right) for 5 trajectories from longer simulation runs of 1000 and 2000 temporal iterations respectively.

**Table A1.** Correlation coefficient as *a priori* metric and root-mean-squared error on the enstrophy fluxes as *a posteriori* metric for different reference models (using the differentiable solver) trained with the "state" or "subgrid" loss function.

	$\rho_{\tau_\omega, \mathcal{M}}$	$\ell_{\text{rms}}(\Pi_Z^{\tau_\omega}, \Pi_Z^{\mathcal{M}})$
$\mathcal{M}_{\text{online}}(\text{ref}, \text{state})$	0.49	<b>0.26</b>
$\mathcal{M}_{\text{online}}(\text{ref}, \text{subgrid})$	<b>0.59</b>	0.81

metrics we use for evaluation are always *a posteriori*-based, while the "subgrid" loss is penalizing an *a priori* criterion. We also note that the "subgrid" loss reference performs better than the DRN-based emulator on the largest scales, as seen in the domain-averaged energy evolution and the smallest wavenumbers of the enstrophy spectrum. This is probably explained by the reference being free from emulator imperfections. To quantitatively measure the performance of each loss on respective *a priori* and *a posteriori* metrics, we reproduce Tables 2 and 3 from (Frezat et al., 2022) in Table A1. Here, it is clear that the "state" and "subgrid" losses performs better on *a posteriori* and *a priori* metrics, respectively. However, the online model with "subgrid" loss still outperforms models trained with the offline strategy, which seems to confirm that stability comes from the learning strategy rather than the loss function.



## Open Research Section

The results can be reproduced from the data, models and associated learning algorithms provided along with the pseudo-spectral quasi-geostrophic code. These will be shortly accessible as a notebook section folder.

## Acknowledgments

This research was supported by the CNRS through the 80 PRIME project, the ANR through Melody and OceaniX. As part of the M2LiNES project, additional support was also provided by Schmidt Futures, a philanthropic initiative founded by Eric and Wendy Schmidt, as part of its Virtual Earth System Research Institute (VESRI). Computations were performed using GPU resources from GENCI-IDRIS.

## References

- Bae, H. J., & Koumoutsakos, P. (2022). Scientific multi-agent reinforcement learning for wall-models of turbulent flows. *Nature Communications*, 13(1), 1443. doi: 10.1038/s41467-022-28957-7
- Baydin, A. G., Pearlmutter, B. A., Radul, A. A., & Siskind, J. M. (2018). Automatic differentiation in machine learning: a survey. *Journal of Machine Learning Research*, 18(153), 1–43.
- Beucler, T., Pritchard, M., Rasp, S., Ott, J., Baldi, P., & Gentine, P. (2021). Enforcing analytic constraints in neural networks emulating physical systems. *Physical Review Letters*, 126(9), 098302. doi: 10.1103/PhysRevLett.126.098302
- Bocquet, M. (2023). Surrogate modeling for the climate sciences dynamics with machine learning and data assimilation. *Frontiers in Applied Mathematics and Statistics*, 9, 1133226. doi: 10.3389/fams.2023.1133226
- Bolton, T., & Zanna, L. (2019). Applications of deep learning to ocean data inference and subgrid parameterization. *Journal of Advances in Modeling Earth Systems*, 11(1), 376–399. doi: 10.1029/2018MS001472
- Bouchet, F., & Venaille, A. (2012). Statistical mechanics of two-dimensional and geophysical flows. *Physics Reports*, 515(5), 227–295. doi: 10.1016/j.physrep.2012.02.001
- Brunton, S. L., Noack, B. R., & Koumoutsakos, P. (2020). Machine learning for fluid mechanics. *Annual Review of Fluid Mechanics*, 52, 477–508. doi: 10.1146/

annurev-fluid-010719-060214

- Canuto, C., Hussaini, M. Y., Quarteroni, A., & Zang, T. A. (2007). *Spectral methods: Fundamentals in single domains*. Springer Science & Business Media.
- Carrassi, A., Bocquet, M., Bertino, L., & Evensen, G. (2018). Data assimilation in the geosciences: An overview of methods, issues, and perspectives. *Wiley Interdisciplinary Reviews: Climate Change*, 9(5), e535. doi: 10.1002/wcc.535
- Cranmer, K., Brehmer, J., & Louppe, G. (2020). The frontier of simulation-based inference. *Proceedings of the National Academy of Sciences*, 117(48), 30055–30062. doi: 10.1073/pnas.1912789117
- Danilov, S., Juricke, S., Kutsenko, A., & Oliver, M. (2019). Toward consistent sub-grid momentum closures in ocean models. *Energy Transfers in Atmosphere and Ocean*, 145–192. doi: 10.1007/978-3-030-05704-6\_5
- Dresdner, G., Kochkov, D., Norgaard, P., Zepeda-Núñez, L., Smith, J. A., Brenner, M. P., & Hoyer, S. (2022). Learning to correct spectral methods for simulating turbulent flows. *arXiv preprint*. doi: 10.48550/arXiv.2207.00556
- Duraisamy, K. (2021). Perspectives on machine learning-augmented reynolds-averaged and large eddy simulation models of turbulence. *Physical Review Fluids*, 6(5), 050504. doi: 10.1103/physrevfluids.6.050504
- Fan, X., & Wang, J.-X. (2024). Differentiable hybrid neural modeling for fluid-structure interaction. *Journal of Computational Physics*, 496, 112584. doi: 10.1016/j.jcp.2023.112584
- Farchi, A., Laloyaux, P., Bonavita, M., & Bocquet, M. (2021). Using machine learning to correct model error in data assimilation and forecast applications. *Quarterly Journal of the Royal Meteorological Society*, 147(739), 3067–3084. doi: 10.1002/qj.4116
- Finn, T. S., Durand, C., Farchi, A., Bocquet, M., Chen, Y., Carrassi, A., & Dansereau, V. (2023). Deep learning of subgrid-scale parametrisations for short-term forecasting of sea-ice dynamics with a maxwell-elasto-brittle rheology. *EGUsphere*, 1–39. doi: 10.5194/egusphere-2022-1342
- Fox-Kemper, B., Adcroft, A., Böning, C. W., Chassignet, E. P., Curchitser, E., Danabasoglu, G., ... others (2019). Challenges and prospects in ocean circulation models. *Frontiers in Marine Science*, 6, 65. doi: 10.3389/fmars.2019.00065
- Fox-Kemper, B., & Menemenlis, D. (2008). Can large eddy simulation techniques

- improve mesoscale rich ocean models? *Washington DC American Geophysical Union Geophysical Monograph Series*, 177, 319–337. doi: 10.1029/177GM19
- Frederiksen, J. S., O’Kane, T. J., & Zidikheri, M. J. (2012). Stochastic subgrid parameterizations for atmospheric and oceanic flows. *Physica Scripta*, 85(6), 068202. doi: 10.1088/0031-8949/85/06/068202
- Frezat, H., Balarac, G., Le Sommer, J., Fablet, R., & Lguensat, R. (2021). Physical invariance in neural networks for subgrid-scale scalar flux modeling. *Physical Review Fluids*, 6(2), 024607. doi: 10.1103/PhysRevFluids.6.024607
- Frezat, H., Le Sommer, J., Fablet, R., Balarac, G., & Lguensat, R. (2022). A posteriori learning for quasi-geostrophic turbulence parametrization. *Journal of Advances in Modeling Earth Systems*, 14(11), e2022MS003124. doi: 10.1029/2022MS003124
- Gelbrecht, M., White, A., Bathiany, S., & Boers, N. (2023). Differentiable programming for earth system modeling. *Geoscientific Model Development*, 16(11), 3123–3135. doi: 10.5194/gmd-16-3123-2023
- Germano, M., Piomelli, U., Moin, P., & Cabot, W. H. (1991). A dynamic subgrid-scale eddy viscosity model. *Physics of Fluids A: Fluid Dynamics*, 3(7), 1760–1765. doi: 10.1063/1.857955
- Graham, J. P., & Ringler, T. (2013). A framework for the evaluation of turbulence closures used in mesoscale ocean large-eddy simulations. *Ocean Modelling*, 65, 25–39. doi: 10.1016/j.ocemod.2013.01.004
- Guan, Y., Chattopadhyay, A., Subel, A., & Hassanzadeh, P. (2022). Stable a posteriori les of 2d turbulence using convolutional neural networks: Backscattering analysis and generalization to higher re via transfer learning. *Journal of Computational Physics*, 458, 111090. doi: 10.1016/j.jcp.2022.111090
- Guan, Y., Subel, A., Chattopadhyay, A., & Hassanzadeh, P. (2023). Learning physics-constrained subgrid-scale closures in the small-data regime for stable and accurate les. *Physica D: Nonlinear Phenomena*, 443, 133568. doi: 10.1016/j.physd.2022.133568
- Guillaumin, A. P., & Zanna, L. (2021). Stochastic-deep learning parameterization of ocean momentum forcing. *Journal of Advances in Modeling Earth Systems*, 13(9), e2021MS002534. doi: 10.1029/2021MS002534
- Heiden, E., Millard, D., Coumans, E., Sheng, Y., & Sukhatme, G. S. (2021). Neural-

- Sim: Augmenting differentiable simulators with neural networks. In *2021 IEEE International Conference on Robotics and Automation (ICRA)* (pp. 9474–9481). doi: 10.1109/ICRA48506.2021.9560935
- Hewitt, H. T., Roberts, M., Mathiot, P., Biastoch, A., Blockley, E., Chassignet, E. P., ... others (2020). Resolving and parameterising the ocean mesoscale in earth system models. *Current Climate Change Reports*, 6, 137–152. doi: 10.1007/s40641-020-00164-w
- Hochreiter, S. (1998). The vanishing gradient problem during learning recurrent neural nets and problem solutions. *International Journal of Uncertainty, Fuzziness and Knowledge-Based Systems*, 6(02), 107–116. doi: 10.1142/s0218488598000094
- Holl, P., Thuerey, N., & Koltun, V. (2020). Learning to control PDEs with differentiable physics. In *International conference on learning representations*.
- Huang, D. Z., Huang, J., Reich, S., & Stuart, A. M. (2022). Efficient derivative-free bayesian inference for large-scale inverse problems. *Inverse Problems*, 38(12), 125006. doi: 10.1088/1361-6420/ac99fa
- Iglesias, M. A., Law, K. J., & Stuart, A. M. (2013). Ensemble kalman methods for inverse problems. *Inverse Problems*, 29(4), 045001. doi: 10.1088/0266-5611/29/4/045001
- Jansen, M. F., Held, I. M., Adcroft, A., & Hallberg, R. (2015). Energy budget-based backscatter in an eddy permitting primitive equation model. *Ocean Modelling*, 94, 15–26. doi: 10.1016/j.ocemod.2015.07.015
- Juricke, S., Danilov, S., Koldunov, N., Oliver, M., & Sidorenko, D. (2020). Ocean kinetic energy backscatter parametrization on unstructured grids: Impact on global eddy-permitting simulations. *Journal of Advances in Modeling Earth Systems*, 12(1), e2019MS001855. doi: 10.1029/2019MS001855
- Juricke, S., Danilov, S., Kutsenko, A., & Oliver, M. (2019). Ocean kinetic energy backscatter parametrizations on unstructured grids: Impact on mesoscale turbulence in a channel. *Ocean Modelling*, 138, 51–67. doi: 10.1016/j.ocemod.2019.03.009
- Kim, J., Kim, H., Kim, J., & Lee, C. (2022). Deep reinforcement learning for large-eddy simulation modeling in wall-bounded turbulence. *Physics of Fluids*, 34(10). doi: 10.1063/5.0106940

- Kochkov, D., Smith, J. A., Alieva, A., Wang, Q., Brenner, M. P., & Hoyer, S. (2021). Machine learning–accelerated computational fluid dynamics. *Proceedings of the National Academy of Sciences*, 118(21), e2101784118. doi: 10.1073/pnas.2101784118
- Kovachki, N. B., & Stuart, A. M. (2019). Ensemble kalman inversion: a derivative-free technique for machine learning tasks. *Inverse Problems*, 35(9), 095005. doi: 10.1088/1361-6420/ab1c3a
- Kravchenko, A., & Moin, P. (1997). On the effect of numerical errors in large eddy simulations of turbulent flows. *Journal of Computational Physics*, 131(2), 310–322. doi: 10.1006/jcph.1996.5597
- Kurz, M., Offenhäuser, P., & Beck, A. (2023). Deep reinforcement learning for turbulence modeling in large eddy simulations. *International Journal of Heat and Fluid Flow*, 99, 109094. doi: 10.1016/j.ijheatfluidflow.2022.109094
- Leonard, A. (1975). Energy cascade in large-eddy simulations of turbulent fluid flows. In *Advances in geophysics* (Vol. 18, pp. 237–248). Elsevier. doi: 10.1016/S0065-2687(08)60464-1
- Lesieur, M., & Metais, O. (1996). New trends in large-eddy simulations of turbulence. *Annual Review of Fluid Mechanics*, 28(1), 45–82. doi: 10.1146/annurev.fl.28.010196.000401
- Lilly, D. K. (1992). A proposed modification of the germano subgrid-scale closure method. *Physics of Fluids A: Fluid Dynamics*, 4(3), 633–635. doi: 10.1063/1.858280
- List, B., Chen, L.-W., & Thuerey, N. (2022). Learned turbulence modelling with differentiable fluid solvers: physics-based loss functions and optimisation horizons. *Journal of Fluid Mechanics*, 949, A25. doi: 10.1017/jfm.2022.738
- Liu, Y., Lu, L., Fang, L., & Gao, F. (2011). Modification of spalart–allmaras model with consideration of turbulence energy backscatter using velocity helicity. *Physics Letters A*, 375(24), 2377–2381. doi: 10.1016/j.physleta.2011.05.023
- Lopez-Gomez, I., Christopoulos, C., Langeland Ervik, H. L., Dunbar, O. R., Cohen, Y., & Schneider, T. (2022). Training physics-based machine-learning parameterizations with gradient-free ensemble kalman methods. *Journal of Advances in Modeling Earth Systems*, 14(8), e2022MS003105. doi: 10.1029/2022ms003105

- MacArt, J. F., Sirignano, J., & Freund, J. B. (2021). Embedded training of neural-network subgrid-scale turbulence models. *Physical Review Fluids*, 6(5), 050502. doi: 10.1103/PhysRevFluids.6.050502
- Maher, P., Vallis, G. K., Sherwood, S. C., Webb, M. J., & Sansom, P. G. (2018). The impact of parameterized convection on climatological precipitation in atmospheric global climate models. *Geophysical Research Letters*, 45(8), 3728–3736. doi: 10.1002/2017gl076826
- Maulik, R., San, O., Rasheed, A., & Vedula, P. (2019). Subgrid modelling for two-dimensional turbulence using neural networks. *Journal of Fluid Mechanics*, 858, 122–144. doi: 10.1017/jfm.2018.770
- McGibbon, J., & Bretherton, C. (2019). Single-column emulation of reanalysis of the northeast pacific marine boundary layer. *Geophysical Research Letters*, 46(16), 10053–10060. doi: 10.1029/2019GL083646
- Meneveau, C., & Katz, J. (2000). Scale-invariance and turbulence models for large-eddy simulation. *Annual Review of Fluid Mechanics*, 32(1), 1–32. doi: 10.1146/annurev.fluid.32.1.1
- Négier, G., Mahoney, M. W., & Krishnapriyan, A. S. (2023). Learning differentiable solvers for systems with hard constraints. In *International conference on learning representations*.
- Nonnenmacher, M., & Greenberg, D. S. (2021). Deep emulators for differentiation, forecasting, and parametrization in earth science simulators. *Journal of Advances in Modeling Earth Systems*, 13(7), e2021MS002554. doi: 10.1029/2021MS002554
- Novati, G., de Laroussilhe, H. L., & Koumoutsakos, P. (2021). Automating turbulence modelling by multi-agent reinforcement learning. *Nature Machine Intelligence*, 3(1), 87–96. doi: 10.1038/s42256-020-00272-0
- Ouala, S., Chapron, B., Collard, F., Gaultier, L., & Fablet, R. (2023). Online calibration of deep learning sub-models for hybrid numerical modeling systems. *arXiv preprint*. doi: 10.48550/arXiv.2311.10665
- Pahlavan, H. A., Hassanzadeh, P., & Alexander, M. J. (2024). Explainable offline-online training of neural networks for parameterizations: A 1d gravity wave-qbo testbed in the small-data regime. *Geophysical Research Letters*, 51(2), e2023GL106324. doi: 10.1029/2023GL106324

- Pawar, S., & San, O. (2021). Data assimilation empowered neural network parametrizations for subgrid processes in geophysical flows. *Physical Review Fluids*, 6(5), 050501. doi: 10.1103/PhysRevFluids.6.050501
- Pawar, S., San, O., Rasheed, A., & Vedula, P. (2020). A priori analysis on deep learning of subgrid-scale parameterizations for kraichnan turbulence. *Theoretical and Computational Fluid Dynamics*, 34, 429–455. doi: 10.1007/s00162-019-00512-z
- Pawar, S., San, O., Rasheed, A., & Vedula, P. (2023). Frame invariant neural network closures for kraichnan turbulence. *Physica A: Statistical Mechanics and its Applications*, 609, 128327. doi: 10.1016/j.physa.2022.128327
- Pedersen, C., Zanna, L., Bruna, J., & Perezhogan, P. (2023). Reliable coarse-grained turbulent simulations through combined offline learning and neural emulation. In *Icml2023 workshop on the synergy of scientific and machine learning modeling*.
- Piomelli, U., Cabot, W. H., Moin, P., & Lee, S. (1991). Subgrid-scale backscatter in turbulent and transitional flows. *Physics of Fluids A: Fluid Dynamics*, 3(7), 1766–1771. doi: 10.1063/1.857956
- Ramadhan, A., Marshall, J., Souza, A., Wagner, G. L., Ponnampati, M., & Rackauckas, C. (2020). Capturing missing physics in climate model parameterizations using neural differential equations. *arXiv preprint*. doi: 10.48550/arXiv.2010.12559
- Rasp, S., Pritchard, M. S., & Gentine, P. (2018). Deep learning to represent subgrid processes in climate models. *Proceedings of the National Academy of Sciences*, 115(39), 9684–9689. doi: 10.1073/pnas.1810286115
- Rogallo, R. S., & Moin, P. (1984). Numerical simulation of turbulent flows. *Annual Review of Fluid Mechanics*, 16(1), 99–137. doi: 10.1146/annurev.fl.16.010184.000531
- Ross, A., Li, Z., Perezhogan, P., Fernandez-Granda, C., & Zanna, L. (2023). Benchmarking of machine learning ocean subgrid parameterizations in an idealized model. *Journal of Advances in Modeling Earth Systems*, 15(1), e2022MS003258. doi: 10.1029/2022MS003258
- Sagaut, P. (2005). *Large eddy simulation for incompressible flows: An introduction*. Springer Science & Business Media.

- Sanchez-Gonzalez, A., Heess, N., Springenberg, J. T., Merel, J., Riedmiller, M., Hassel, R., & Battaglia, P. (2018). Graph networks as learnable physics engines for inference and control. In *Proceedings of the 35th international conference on machine learning* (pp. 4470–4479).
- Schneider, T., Lan, S., Stuart, A., & Teixeira, J. (2017). Earth system modeling 2.0: A blueprint for models that learn from observations and targeted high-resolution simulations. *Geophysical Research Letters*, 44(24), 12–396. doi: 10.1002/2017gl076101
- Schumann, U. (1995). Stochastic backscatter of turbulence energy and scalar variance by random subgrid-scale fluxes. *Proceedings of the Royal Society of London. Series A: Mathematical and Physical Sciences*, 451(1941), 293–318. doi: 10.1098/rspa.1995.0126
- Seifert, A., & Rasp, S. (2020). Potential and limitations of machine learning for modeling warm-rain cloud microphysical processes. *Journal of Advances in Modeling Earth Systems*, 12(12), e2020MS002301. doi: 10.1029/2020MS002301
- Shankar, V., Puri, V., Balakrishnan, R., Maulik, R., & Viswanathan, V. (2023). Differentiable physics-enabled closure modeling for burgers’ turbulence. *Machine Learning: Science and Technology*, 4(1), 015017. doi: 10.1088/2632-2153/acb19c
- Sirignano, J., & MacArt, J. F. (2023). Dynamic deep learning les closures: Online optimization with embedded dns. *arXiv preprint*. doi: 10.48550/arXiv:2303.02338
- Sirignano, J., MacArt, J. F., & Freund, J. B. (2020). DPM: A deep learning pde augmentation method with application to large-eddy simulation. *Journal of Computational Physics*, 423, 109811. doi: 10.1016/j.jcp.2020.109811
- Smagorinsky, J. (1963). General circulation experiments with the primitive equations: I. the basic experiment. *Monthly Weather Review*, 91(3), 99–164. doi: 10.1175/1520-0493(1963)091<0099:GCEWTP>2.3.CO;2
- Stachenfeld, K., Fielding, D. B., Kochkov, D., Cranmer, M., Pfaff, T., Godwin, J., ... Sanchez-Gonzalez, A. (2022). Learned coarse models for efficient turbulence simulation. In *International conference on learning representations*.
- Takahashi, T., Liang, J., Qiao, Y.-L., & Lin, M. C. (2021). Differentiable fluids



- with solid coupling for learning and control. In *Proceedings of the aaai conference on artificial intelligence* (Vol. 35, pp. 6138–6146). doi: 10.1609/aaai.v35i7.16764
- Thompson, A. F. (2010). Jet formation and evolution in baroclinic turbulence with simple topography. *Journal of Physical Oceanography*, 40(2), 257–278. doi: 10.1175/2009JPO4218.1
- Um, K., Brand, R., Fei, Y. R., Holl, P., & Thuerey, N. (2020). Solver-in-the-loop: Learning from differentiable physics to interact with iterative PDE-solvers. In *Advances in neural information processing systems* (Vol. 33, pp. 6111–6122).
- Vinuesa, R., & Brunton, S. L. (2022). Enhancing computational fluid dynamics with machine learning. *Nature Computational Science*, 2(6), 358–366. doi: 10.1038/s43588-022-00264-7
- Wagner, G. L., Hillier, A., Constantinou, N. C., Silvestri, S., Souza, A. N., Burns, K., ... others (2023). CATKE: a turbulent-kinetic-energy-based parameterization for ocean microturbulence with dynamic convective adjustment. *Authorea Preprints*.
- Watt-Meyer, O., Brenowitz, N. D., Clark, S. K., Henn, B., Kwa, A., McGibbon, J., ... Bretherton, C. S. (2021). Correcting weather and climate models by machine learning nudged historical simulations. *Geophysical Research Letters*, 48(15), e2021GL092555. doi: 10.1029/2021GL092555
- Yang, Y., Robinson, C., Heitz, D., & M  min, E. (2015). Enhanced ensemble-based 4dvar scheme for data assimilation. *Computers & Fluids*, 115, 201–210. doi: 10.1016/j.compfluid.2015.03.025
- Yuval, J., & O’Gorman, P. A. (2020). Stable machine-learning parameterization of subgrid processes for climate modeling at a range of resolutions. *Nature communications*, 11(1), 3295. doi: 10.1038/s41467-020-17142-3